Journal of
Materials Chemistry C
Materials for optical, magnetic and electronic devices

This article can be cited before page numbers have been issued, to do this please use: B. Sk, S. Sharma, A. James, S. Kundu and A. Patra, *J. Mater. Chem. C*, 2020, DOI: 10.1039/D0TC02520H.

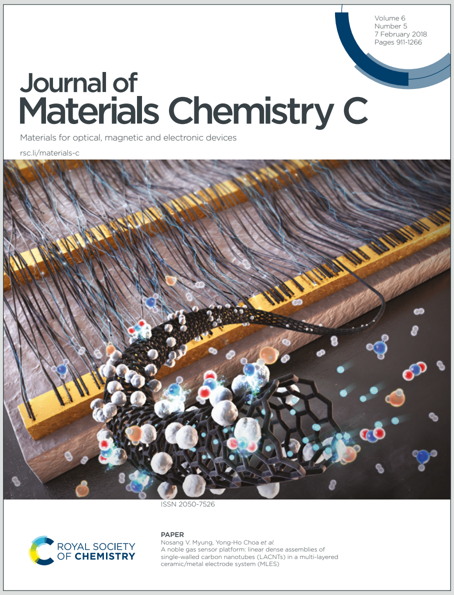

View Article Online
DOI: 10.1039/D0TC02520H

N-rich electron acceptors: triplet harvesting in multichromophoric pyridoquinoxaline and pyridopyrazine-based organic emitters

Received 00th January 20xx,
Accepted 00th January 20xx

DOI: 10.1039/x0xx00000x

Bahadur Sk,[a] Samarth Sharma,[a] Anto James,[a,b] Subhankar Kundu,[a] and Abhijit Patra*[a]

Controlling the nonradiative deactivation of triplet states and tuning the singlet-triplet energy gap are the major challenges to develop materials exhibiting thermally activated delayed fluorescence (TADF) and room temperature phosphorescence (RTP). Additionally, the conformational flexibility/ rigidity around the donor-acceptor bond and π-spacer unit significantly alters the charge transfer efficiency, subsequently impacting the relative propensity of TADF and RTP. Herein, we propose a new class of multichromophoric tridonor-acceptor (D_3-A) compounds with rigid and flexible π-spacer having N-rich pyridoquinoxaline and pyridopyrazine acceptor core, respectively. The molecule with carbazole donors at *meta* to quinoxaline nitrogen of rigid pyridoquinoxaline core exhibits TADF. Whereas, the variation of the linkage position of carbazole to pyridoquinoxaline as well as twisted and flexible pyridopyrazine core show predominantly RTP due to relatively higher singlet-triplet energy gap. Increasing the donor strength with phenoxazine in pyridopyrazine system leads to TADF and RTP simultaneously. Further, we demonstrate the promising scope of all-organic triplet harvesting materials in solid-state security encryption.

Introduction

Smart organic donor-acceptor (D-A) based multichromophores have gained profound interest in recent years owing to the efficient harvesting of the triplet excited states.[1-9] The triplet state could be emissive by thermally activated delayed fluorescence (TADF) or the radiative decay at ambient conditions, commonly known as room temperature phosphorescence (RTP).[10-15] Such emitters are making their way in a wide variety of photonics applications like organic light-emitting diodes (OLEDs),[2,16] sensors,[17] security devices,[18-20] time-resolved luminescence imaging,[21,22] etc. The key challenges are to control the dynamic collisional quenching of triplet excited state and lowering the energy gap between the excited singlet (S_1) and triplet (T_1) states (ΔE_{ST}).[18,23-26] The lower ΔE_{ST} value promotes the photon upconversion from excited triplet states to the emissive singlet states through reverse intersystem crossing (RISC) leading to TADF.[2] The excited-state intramolecular charge transfer (ICT) in donor-acceptor (D-A) molecules with spatially-separated the highest occupied molecular orbitals (HOMOs) and the lowest unoccupied molecular orbitals (LUMOs) is conducive to low ΔE_{ST} values.[2] The charge transfer interactions also favour a strong spin-orbit coupling (SOC) through the mixing of singlet and triplet electronic excited states.[27,28] Consequently, a high rate of intersystem crossing (ISC) along with stable triplet excited states leads to persistent or ultralong RTP in certain D-A compounds.[18,24,29]

The charge transfer interactions depend not only on the molecular geometry but also vary with the relative orientation of donor and acceptor units.[8,30-33] ICT significantly differs among positional isomers with different substitution positions of donors on the acceptor core.[34] Chen *et al.* demonstrated the switching between TADF and RTP in phenothiazine-benzophenone based D-A compounds invoking the concept of twisted intramolecular charge transfer (TICT) and planarized intramolecular charge transfer (PICT).[8] Bryce and coworkers observed RTP in phenothiazine–dibenzothiophene-S,S-dioxide based D-A-D pair by introducing steric hindrance on the donor units.[12] Tunable delayed emission from green to red by increasing the number of donor units from D-A, D_2-A, to D_3-A architecture by controlling the ICT effect was demonstrated by Xie et al.[35] As reported by Reineke and coworkers, additional nitrogen atoms enhance the SOC, and subsequently, the rate of ISC.[13] Amidst several recent reports, a unified molecular design strategy unraveling the abstruse role of the N-rich central acceptor core along with conformational analysis in multichromophoric organic emitters for tunable and efficient TADF and RTP is still intriguing albeit challenging.

Herein, we have examined the role of N-rich acceptor units along with π-spacers in terms of flexibility/ rigidity and twisted/ planar geometry on emission properties of D_3-A molecules at different timescale. The central core of pyridoquinoxaline and pyridopyrazine serve as facile acceptor units owing to the multiple nitrogen centers, which also favor the ISC (Fig. 1, Table

---

[a] *Department of Chemistry, Indian Institute of Science Education and Research Bhopal, Bhauri, Bhopal, Madhya Pradesh, 462066, India.*
E-mail: abhijit@iiserb.ac.in
[b] *Department of Chemistry, Indian Institute of Science Education and Research Thiruvananthapuram Maruthamala PO, Vithura, Kerala 695551, India.*

† Electronic Supplementary Information (ESI) available: Details of synthesis and characterization, fluorescence decays, time-resolved emission spectra, crystal structure and computational investigations, and supporting videos for RTP. See DOI: 10.1039/x0xx00000x

View Article Online
DOI: 10.1039/D0TC02520H

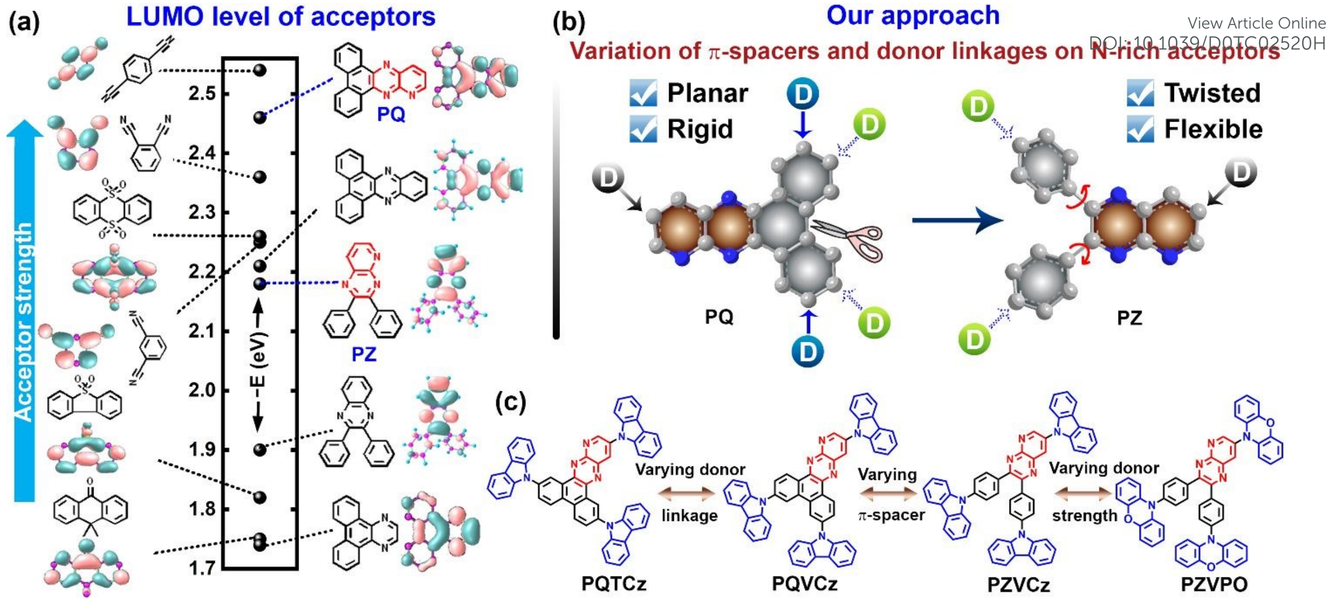

Fig. 1 Design strategy of triplet harvesting materials: (a) a comparative account of the intrinsic electron-accepting capability (LUMO level) of various acceptor units used for triplet harvesting including the new acceptor cores of dibenzopyridoquinoxaline (PQ) and diphenylpyridopyrazine (PZ), estimated employing density functional theory (DFT) at the B3LYP/6-31G(d,p) level. (b) Schematic illustration of our approach representing planar dibenzopyridoquinoxaline (T-shaped: PQT and V-shaped: PQV) and twisted diphenylpyridopyrazine (PZV) acceptor units, and (c) the molecular structures of tridonor-acceptor (D_3-A) compounds with carbazole (Cz) and phenoxazine (PO) as donor units: PQTCz, PQVCz, PZVCz and PZVPO; D-A linkage, π-spacer, and donor strength are varied.

S1, S2, ESI†). Furthermore, the adjacent phenyl spacers also offer a distinctive synthetic advantage in regulating the molecular flexibility/ rigidity of the central core. The molecule with carbazole donors at *meta* to quinoxaline nitrogen of rigid pyridoquinoxaline core showed enhanced TADF due to the low ΔE_{ST}. However, the higher ΔE_{ST} due to variation of the linkage position of carbazole (*para* to quinoxaline nitrogen) to pyridoquinoxaline and pyridopyrazine core resulted in predominant RTP. The simultaneous TADF and RTP were achieved employing phenoxazine as donors in pyridopyrazine system.

Results and discussion

Quinoxaline is a well-known electron acceptor unit due to the presence of two electronegative sp^2 hybridized nitrogen atoms.[36-38] Phenazine also possesses similar electron-deficient characteristics as quinoxaline.[39,40] The presence of another nitrogen-containing heterocycle to the quinoxaline unit leads to the pyridoquinoxaline motif, with better electron accepting capability than quinoxaline or phenazine (Table S1, ESI†). Similarly, pyridopyrazine is more electron deficient than pyrazine (Table S1, ESI†). The suitable inclusion of π-spacers (phenyl groups) leads to the development of dibenzopyridoquinoxaline and diphenylpyridopyrazine (Fig. 1a, b). The phenyl π-spacers do not alter the electron-withdrawing capabilities of pyridoquinoxaline or pyridopyrazine, rather allow synthetic flexibility and a range of viable options to introduce the donor substituents. Henceforth, dibenzopyridoquinoxaline and diphenylpyridopyrazine are abbreviated as PQ and PZ, respectively. The significant difference between PQ and PZ core lies in the molecular flexibility/ rigidity induced by the linkage pattern of phenyl spacers (Fig. 1b). Donor substitutions at 2,7 and 3,6-positions of PQ lead to T and V-shaped molecular geometry.[34]

We introduce multiple electron donor units covalently linked with central PQ and PZ core for the development of a new series of multichromophoric D_3-A molecules. Considering the efficient electron-donating properties, high thermal stability and low-cost, carbazole and phenoxazine were chosen as the donor units.[41] Palladium-catalyzed Buchwald-Hartwig cross-coupling reactions (C-N coupling) of tribromo-PQT, PQV, and PZV with carbazole and phenoxazine resulted in PQTCz, PQVCz, PZVCz, and PZVPO (Fig. 1c, Scheme 1, S1-S6, ESI†). All the compounds were characterized by NMR spectroscopic and mass spectrometric analysis (Fig. S48-S70, ESI†).

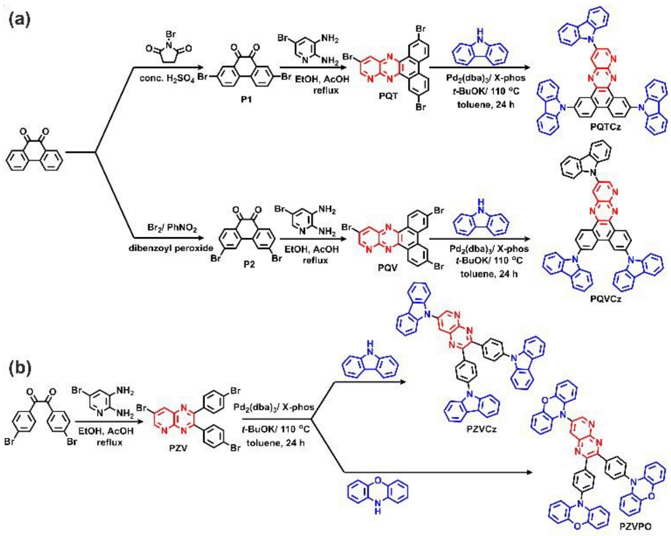

Scheme 1 Schematic illustration for synthetic pathways of (a) pyridoquinoxaline based PQTCz, PQVCz, and (b) pyridopyrazine based PZVCz and PZVPO compounds.

View Article Online
DOI: 10.1039/D0TC02520H

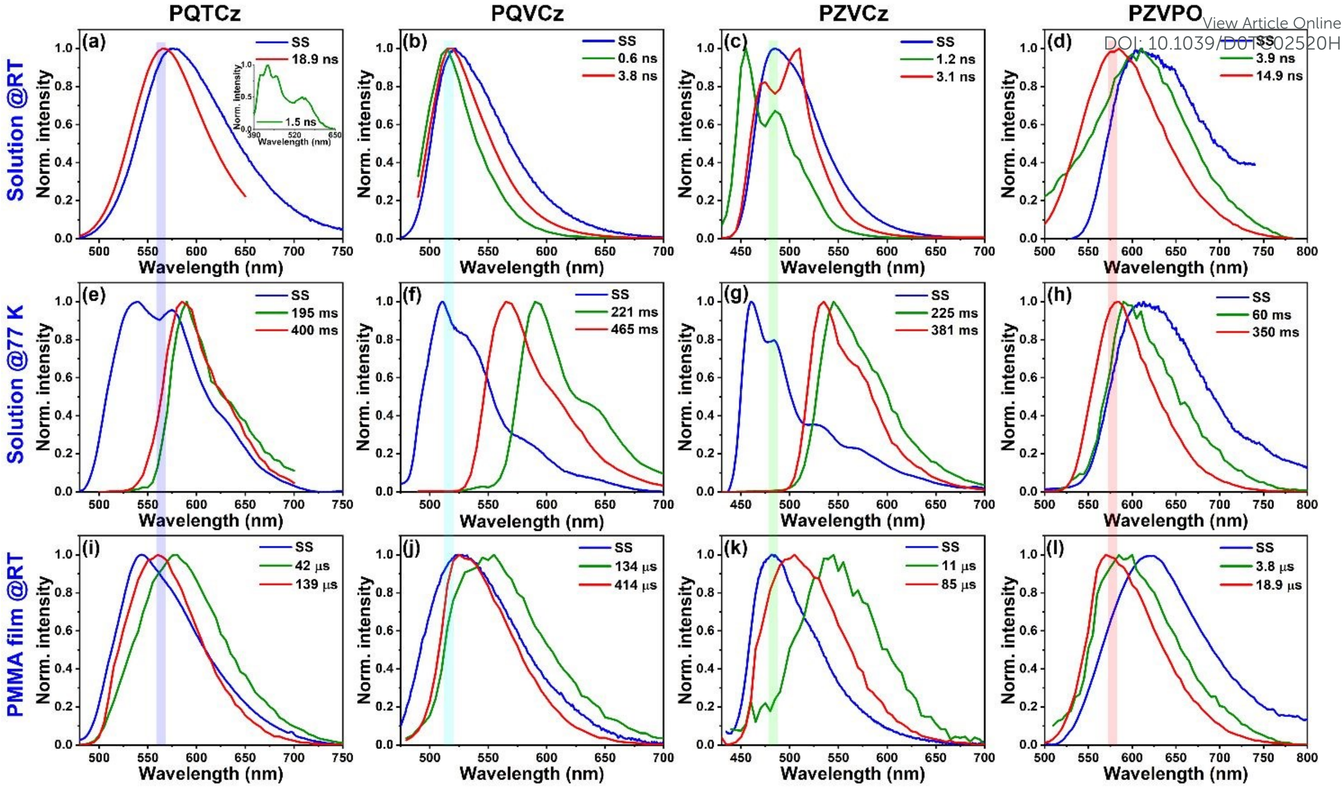

Fig. 2 Time-resolved emission spectra (TRES) from nanosecond to millisecond timescale: normalized emission spectra of D_3-A compounds in toluene at room temperature (a-d), in toluene at 77 K (e-h) and in polymethyl methacrylate (PMMA) films at room temperature (RT: 22-25°C, i-l), respectively for (a, e, i) PQTCz (a Inset: spectrum at 1.5 ns depicting locally excited state (LE) emission), (b, f, j) PQVCz, (c, g, k) PZVCz, and (d, h, l) PZVPO. Spectra were recorded using λ_{ex} = 465 nm [steady state (SS), 450 W Xe lamp], λ_{ex} = 468 nm [picosecond (ps) diode laser] and 461 nm [millisecond (ms) multi-channel scanning (MCS) spectraLED] for PQTCz, PQVCz and PZVPO, respectively and λ_{ex} = 420 nm (SS, 450 W Xe lamp), λ_{ex} = 410 nm (ps diode laser) and 417 nm (ms MCS spectraLED) for PZVCz. The solid bars indicate the similarity of emission peak positions of D_3-A compounds at different timescale in solution at RT, 77K, and in polymer film.

D_3-A compounds absorb predominantly in the UV-region along with a prominent broad absorption band in the visible region (Fig. S1, S2, ESI†). The lower-energy absorption bands are attributed to the extended π-conjugation between the donor and the acceptor units.[34,42,43] Whereas, the higher energy absorption bands are ascribed to π-π* transitions. Strong fluorescence with broad emission bands was observed for PQTCz, PQVCz, and PZVCz in toluene (5 μM) at room temperature (Fig. 2a-c, Table S4-S7, ESI†). A relatively weak emission was noticeable for PZVPO in toluene at room temperature (Fig. 2d, strong D-A pair, dark TICT, *vide infra*).[34,42] On increasing the solvent polarity from toluene to dichloromethane, a gradual bathochromic shift in the emission maxima was observed for all compounds (Fig. S4, Table S4, ESI†). The emission maxima were found to be independent of the excitation wavelengths (Fig. S5, ESI†). The spectral broadening of the emission bands with increasing solvent polarity and positive solvatochromic behaviour are the two characteristic features indicative of strong ICT in the D_3-A compounds.[34,42,44,45] Notably, the Stokes shift in PQTCz (*m*-substitution) is higher than PQVCz and PZVCz (*p*-substitution) in all solvents (Table S5-S7, ESI†), which is in agreement with the more facile ICT in the former.[34] The largest Stokes shift (5245 cm^{-1}, toluene) exhibited by PZVPO among the D_3-A compounds suggests the efficient charge transfer interactions due to stronger donor capacity of phenoxazine over carbazole (Table S2, ESI†). The Lippert-Mataga plots, as shown in Fig. S7, ESI†, further substantiate the ICT behaviour (Table S4, ESI†).

The fluorescence decays were measured in the solvents of varying polarity. A biexponential fluorescence decay for all the compounds at ambient conditions is possibly due to the emission from the locally excited (LE) and the charge transfer state (Fig. S8, Table S5-S7, ESI†).[42,46] Further, the emission decays at 350 to 750 nm with an interval of 5 nm were measured to obtain the decay associated emission spectra for a particular timescale. The reconstructed time-resolved emission spectra (TRES) of PQTCz at 1.5 ns and 18.9 ns show two distinct spectral profiles (Fig. 2a). The emission spectrum obtained at 1.5 ns is similar to that of carbazole emission in toluene (Fig. 2a, S9, 10, ESI†). It refers to the LE emission.[46] The emission at 18.9 ns resembles the steady-state emission and is attributed to the charge transfer fluorescence (Fig. 2a, S9, ESI†). Similarly, the TRES of PQVCz, PZVCz, and PZVPO in toluene at ambient conditions are shown in Fig. 2b-d (Fig. S11-13, section V, ESI†).

The phosphorescence spectra and associated decays of D_3-A compounds were recorded at an ultralow temperature in liquid nitrogen (77 K) using 450 W Xe lamp [steady-state (ss)], picosecond (ps) diode laser and millisecond (ms) multi-channel scanning (MCS) spectraLED as the excitation source. The steady-state spectra of D_3-A compounds at 77 K showed emission bands with multiple humps (Fig. 2e-h) and were significantly different compared to those obtained at room temperature

View Article Online
DOI: 10.1039/D0TC02520H

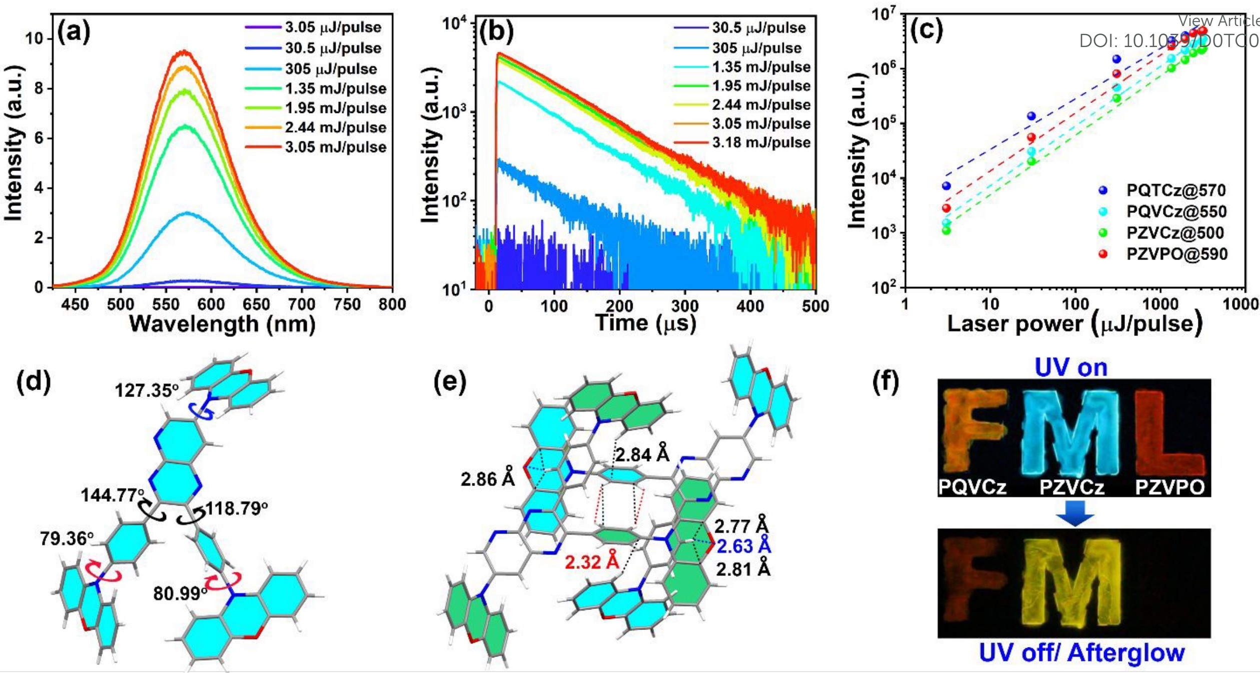

Fig. 3 (a) Emission spectra with varying laser power (pulse width = 5 - 7 ns) of PMMA films of PQTCz at ambient conditions. Spectra were recorded using intensified charge-coupled device (iCCD) camera (λ_{ex} = 355 nm). (b) The emission decay kinetics (λ_{ex} = 355 nm, λ_{em} = 570 nm) of PQTCz-PMMA film with varying laser power at ambient conditions. (c) The linear fitting of the emission intensity of PMMA films of D_3-A compounds as a function of excitation power. (d) The molecular structure of PZVPO obtained from the single crystal X-ray diffraction analysis; significant dihedral angles depicting twisted geometry. (e) The intra- and intermolecular interactions in a single crystal of PZVPO; the strong intermolecular C–H···O interactions (2.63-2.86 Å) between the phenoxazine oxygen and CH of π-spacer phenyl group is indicated. The dimer of PZVPO is further stabilized by the intermolecular interactions between the π-spacer phenyl groups [CH···HC, 2.32 Å, CH···π, 2.84 Å; grey (C), blue (N), red (O). (f) The digital images of PQVCz, PZVCz, and PZVPO-doped PMMA films at room temperature under the excitation of UV-lamp (λ_{ex} = 365 nm), and the photographs after instant turning off the UV irradiation.

(Fig. 2a-d). The biexponential emission decays at 77 K at fast timescale were similar to that observed at room temperature due to the fluorescence from LE and charge transfer states (Fig. 2a-d, S15a-S18a, ESI†). However, the decay measurements at slower timescale at 77 K revealed ultralong phosphorescence ranging from few milliseconds to 0.5 seconds (Fig. 2e-h, Fig. S15b-S18b, ESI†).

The phosphorescence emission maxima of PQTCz were observed at 585 and 590 nm with decay time 400 and 195 ms, respectively (Fig. 2e, S15b, ESI†). PQVCz emits with peaks at 565 and 590 nm with decay time 465 and 221 ms, respectively (Fig. 2f, S16b, ESI†). The phosphorescence emission peak maxima of PZVCz were noticeable at 535 and 545 nm with decay time 381 and 225 ms, respectively (Fig. 2g, S17b, ESI†). The phosphorescence decay time of PZVPO is 350 and 60 ms with a peak centered at 585 and 595 nm, respectively (Fig. 2h, S18b, ESI†), which are very close to the fluorescence bands observed in toluene at room temperature (585 and 610 nm, Fig. 2d). The multiexponential phosphorescence decays suggest more than one triplet charge-transfer state (^{3}CT) due to the presence of multiple donor units.[12] The lower ΔE_{ST} values (<0.5 eV) of D_3-A compounds based on experimental data indicate the possible thermally activated RISC (Fig. S20, Table S8, ESI†). The long-lived emission decay at room temperature with the oxygen-free condition of D_3-A compounds in toluene revealed the prominent delayed emission characteristics of PQTCz (Fig. S21, S22, ESI†). However, no longer component emission was observed for PQVCz, PZVCz, and PZVPO under the same conditions.

We doped the D_3-A compounds in the polymethyl methacrylate (PMMA) matrix to ascertain the triplet harvesting characteristics in the rigid media. PMMA films of all the compounds emit (steady-state) in the distinct regions of the visible spectrum (Fig. 2i-l), ranging from cyan (PZVCz) to green (PQTCz and PQVCz) to red (PZVPO). The decays at the nanosecond timescale monitored at the emission maxima indicate multiple emitting species at room temperature (Fig. S26a-S29a, ESI†). It could be due to the emission from the singlet (LE, ICT), triplet (T_1) states, and aggregates (Fig. S25, Table S10, ESI†).[13,18,25,47] PQTCz film at ambient conditions exhibits emission peaks at 565 and 580 nm, with the decay time 139 and 42 μs, respectively (Fig. 2i, S26b, ESI†). The emission maximum at 565 nm obtained at μs timescale matches with the TRES at room temperature in toluene (18.9 ns), indicating TADF in polymer film (Fig. 2i and 2a). The TRES measured using sensitive gated intensified charge-coupled device (iCCD) camera further ascertain the TADF of PQTCz film (Fig. 3a, S31a, ESI†).[8,48] Unlike the toluene solution at ambient conditions or 77 K, PQVCz film displays distinct longer component emission at 525 and 550 nm with the decay time 414 and 135 μs, respectively demonstrating RTP (Fig. 2j, S27b, S30, ESI†).

We anticipated that the D_3-A compounds with flexible PZ core would exhibit long-lived emission. The peaks at 510 and 545 nm with a respective decay time of 85 and 11 μs of PZVCz film (Fig. 2k, S28b, ESI†) resemble with phosphorescence peaks at 77 K (Fig. 2g). Thus, PZVCz in PMMA film exhibits RTP. Similarly, PZVPO film shows long-lived decays with peaks at 570 and 590 nm having decay time 18.9 and 3.8 μs, respectively (Fig.

View Article Online
DOI: 10.1039/D0TC02520H

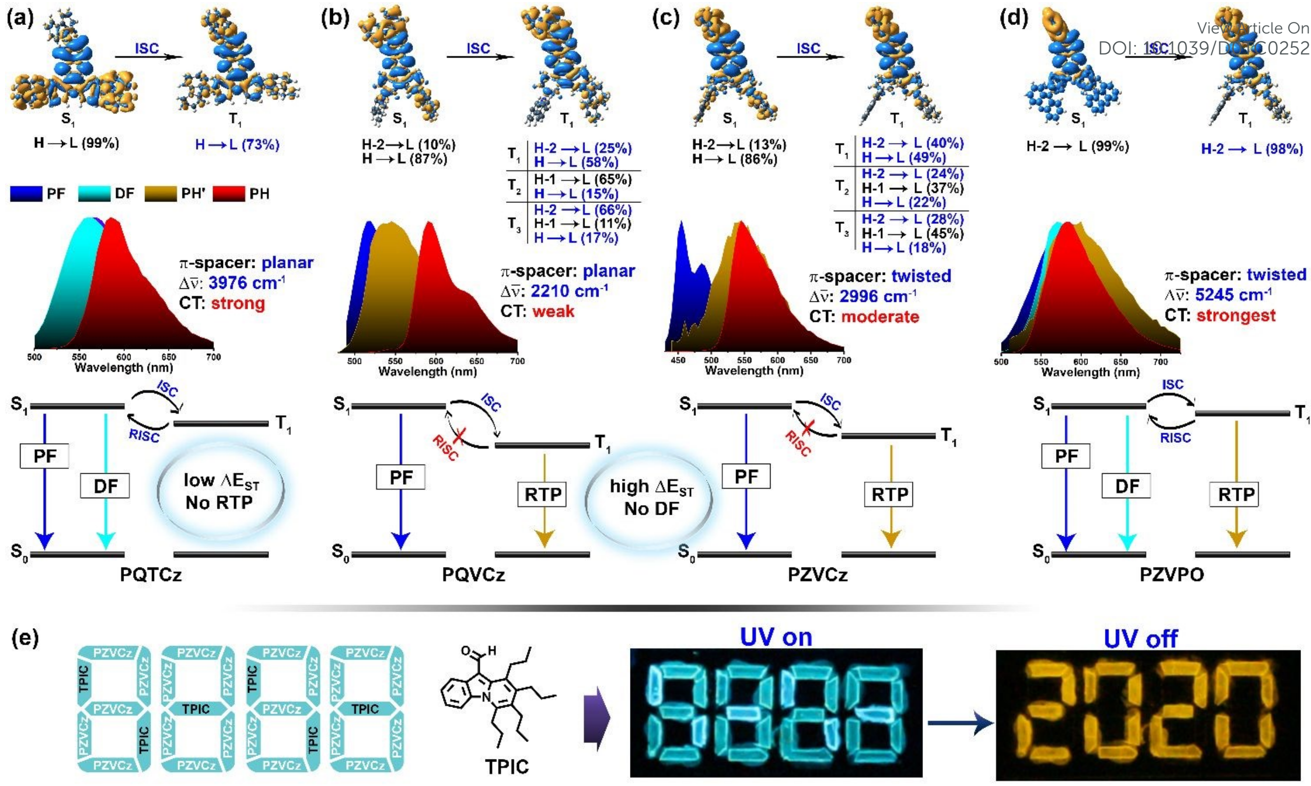

Fig. 4 Molecular-level picture of triplet harvesting in D_3-A compounds: (a) PQTCz, (b) PQVCz, (c) PZVCz, and (d) PZVPO. The TDDFT-calculated electron density differences in the S_1 and T_n states with an isosurface (± 0.0004) and ISC channels involving T_n states with the same transition configurations as in S_1 (blue) within the energy range of $E_{S1} \pm 0.3$ eV are shown. H and L represent the highest occupied molecular orbital (HOMO) and the lowest unoccupied molecular orbital (LUMO), respectively. Normalized emission spectra, and schematic energy profile diagrams of D_3-A compounds; the prompt fluorescence (PF), delayed fluorescence (DF), phosphorescence (PH at 77K) and room temperature phosphorescence (RTP denoted as PH') are displayed. (e) Demonstration of timescale encoding for security application of PZVCz-embedded PMMA film in combination with a cyan emitting 6,7,8,9-tetrapropylpyrido[1,2-*a*]indole-10-carbaldehyde (TPIC, τ~10 ns) fluorophore. On excitation (λ_{ex} = 365 nm), the patterned security feature is unrecognizable due to the strong cyan fluorescence from TPIC and PZVCz. The encrypted feature of '2020' constructed with phosphorescent PZVCz can be identified easily by the naked eye after the excitation is switched off; photographs were captured using a Canon EOS camera with 18-55 mm lens.

2l, S29b, ESI†). Further, the laser power-dependent emission spectra using iCCD camera and decays were recorded to elucidate the long-lived components of D_3-A compounds in a rigid polymer matrix (Fig. 3a, 3b, S32-S35, ESI†). A linear correlation of emission intensity with laser power for all the compounds signifies the unimolecular decay processes (Fig. 3c), ruling out the triplet-triplet annihilation. The long-lived decay in PZVPO film at ambient conditions considering crystal structure analysis (Fig. 3d, 3e), and quantum chemical calculations is presumably due to mixed RTP and delayed fluorescence (*vide infra*).

Tunable fluorescence and RTP with the afterglow feature of D_3-A compounds in polymer films were demonstrated through the encryption of FML (Fig. 3f, written using PQVCz: F, PZVCz: M, and PZVPO: L). Greenish- orange, cyan, and red fluorescence to yellowish-red, yellowish-green, and very weak red RTP, were observed, respectively, from PQVCz, PZVCz, and PZVPO embedded PMMA films (Fig. 3f). The fascinating observations, as mentioned above, were rationalized through time-dependent density functional theory (TDDFT) calculations, coupled with crystal structure investigations (Fig. 3d, 3e, 4a-d, S38-45, Table S12-S16, ESI†). The plots of electron density differences of excited singlet (S_1) and triplet (T_n) states with respect to the ground state (S_0) are shown in Fig. 4a-4d. The electron density shifts from the orange region to the cyan region while the transition from S_0 to S_1 or T_1 states. Additionally, the plots of electron density differences between S_1 and T_1 states indicate that varied distribution of electron density in donors and acceptor units of PQTCz, PQVCz, and PZVCz (Fig. S44a, ESI†). Whereas no such electron density differences were observed for PZVPO (Fig. S44a, ESI†). Because the singlet and triplet states are distributed throughout the molecule in PZVPO (Fig. S44a, S44b, ESI†). The molecular orbitals involved in various electronic transitions within the energy range of $E_{S1} \pm 0.3$ eV and their contributions are shown in Fig. 4a-4d (*vide infra*). Further, the natural transition orbital (NTO) analysis was carried out to comprehend the electronic transitions.[49] There was no direct overlap between the highest occupied natural transition orbitals (HONTOs) and the lowest unoccupied natural transition orbitals (LUNTOs) of D_3-A molecules at S_1 and T_1 states (Fig. S45, ESI†). The results indicate the facile excited-state charge transfer in D_3-A molecules, as suggested by Chen and coworkers.[49] Thus, the similar nature of isosurfaces and transition configurations of excited singlet and triplet states of D_3-A compounds allow facile spin-orbit coupling leading to intersystem crossing (Fig 4a-d).

It is evident that the incorporation of multiple N atoms favors spin-forbidden singlet-triplet transitions according to El-Sayed's rule.[8,23] The computed energy levels of the lowest singlet (E_{S_1}= 2.12 eV) and triplet (E_{T_1} = 1.99 eV) excited states

View Article Online
DOI: 10.1039/D0TC02530H

of PQTCz are very close to the values obtained from the experimental data (Fig. 4a, S20, Table S8, S14, ESI†). The lower ΔE_{ST} (0.13 eV) due to the strong contribution from the charge transfer excitations featuring the decoupled HOMO-LUMO levels enables the photon upconversion through RISC (Fig. 4a, S38, S43, ESI†). Thus, a prominent TADF was observed in the PQTCz film. Whereas, a higher ΔE_{ST} (0.29 eV) and a greater number of energy transition channels (S_1 to T_1, T_2, and T_3) were observed for PQVCz leading to phosphorescence at ambient conditions (Fig. 4b, S39, S43, Table S15, ESI†). Similarly, PZVCz exhibits higher ΔE_{ST} (0.26 eV) and multiple ISC channels between S_1 and T_n (Fig. 4c, S40, S43, Table S15, ESI†), and phosphorescence was observed from PZVCz film.

The molecular structure of PZVPO obtained from crystal structure analysis revealed a highly twisted geometry (Fig. 3d, S46, Table S13, S16, ESI†). The dihedral angles between the central PZ core and the phenyl linker groups are 144.77° and 118.79°, while the dihedral angle between the π-spacers and phenoxazine donor unit is close to 80°. The donor units are connected directly to the acceptor core exhibiting a dihedral angle of 127.35°. Furthermore, a pair of CH···π (2.84 Å) and CH···HC (2.32 Å) intermolecular interactions between π-spacer aromatic phenyl groups generate a dimer like twisted structure along *a* axis (Fig. 3e). These strong intermolecular interactions in the crystals of PZVPO could reduce energy loss through nonradiative relaxation channels.[20,50-52] Additionally, like PQTCz, the similar nature of transition configurations and isosurfaces of S_1 and T_1 in PZVPO increase the probability of ISC leading to high triplet yield (Fig. 4a, 4d, S43, Table S15, ESI†).[15,27,53,54]

The DFT-optimized excited-state structures of both PZVCz and PZVPO indicate the twisted geometry (Table S13, ESI†). A partial twist in the excited-state structure of PZVCz with the dihedral angles 57°, -123°, and -135° was observed for π1-D1, π2-D2, and PZ-D3, respectively. Whereas a more twisted and near orthogonal D-A geometry was observed for PZVPO in the excited state with the dihedral angles 91°, 91°, and -91° for π1-D1, π2-D2, and PZ-D3, respectively (Table S13, ESI†). The introduction of the strong donor phenoxazine in PZVPO led to more twisted structure and small ΔE_{ST} as compared to carbazole based PZVCz.[55] Similarly, the large twist angle in phenoxazine based D-A pair as compared to carbazole as a donor was reported by Oi and coworkers.[56] Further, the twisted structure of PZVPO is due to the steric hindrance of the hydrogen atoms at 1- and 9-positions of phenoxazine (Scheme S7). Whereas, the steric factor is less effective in the case of hydrogens at 1- and 8-positions of carbazole in PZVCz.[56] Thus, the very low ΔE_{ST} value (0.02 eV) owing to the strong charge transfer interactions coupled with long-lived triplet state contributed to the delayed fluorescence and radiative triplet emission in the rigid matrix at ambient conditions in PZVPO (Fig. 4d, S36d, Table S14, ESI†). Temperature-dependent steady-state and time-resolved emission spectra analysis unambiguously ascertain the long-lived decay processes of D_3-A compounds (Fig. 4a-d, S36, S37, Table S11, ESI†).[16,57]

Further, we developed a facile information encryption pattern employing PZVCz thin film along with a cyan emitting dye, 6,7,8,9-tetrapropylpyrido[1,2-*a*]indole-10-carbaldehyde (TPIC) under ambient conditions (Fig. 4e). TPIC exhibits similar strong fluorescence (λ_{max} = 490 nm, τ ~ 10 ns) as that of PZVCz without having any long-lived decay components.[58] The color-changing events were recorded using an image capturing Canon EOS camera (Fig. S47, ESI†). The film upon UV irradiation (λ_{ex} = 365 nm) showed intense cyan fluorescence. A distinctly contrasting greenish-yellow phosphorescence of PZVCz was observed by the naked eye after turning off the UV light source (Fig. 4e, S47, ESI†). Thus, the encrypted information ('2020') from PZVCz is visible multiple times through switching on/off the UV light (see video file, ESI†).

Conclusions

In summary, we developed a new class of multichromophoric tridonor-acceptor compounds with rigid and flexible π-spacers based on pyridoquinoxaline and pyridopyrazine acceptor core, respectively. A strategy for tuning the thermally activated delayed fluorescence and room temperature phosphorescence by controlling the charge transfer interactions through the variation of molecular geometry, as well as the relative orientation of donor and acceptor units, was demonstrated. Strong charge transfer and the lower singlet-triplet energy gap upon the *m*-substitution of donors on rigid pyridoquinoxaline core facilitate reverse intersystem crossing leading to delayed fluorescence. Whereas, the relatively weaker charge transfer and low lying stable triplet states by the *p*-substitution of donors on both pyridoquinoxaline and flexible pyridopyrazine acceptor core, led to predominantly room temperature phosphorescence (Table S17, ESI†). The potential afterglow feature of D_3-A compounds was shown for real-time security data encryption and identification. The present study elucidating the subtle role of donor-acceptor linkages coupled with the rigidity and flexibility of the new N-rich central acceptor cores lays a promising foundation for further development of all-organic materials for triplet harvesting.

Conflicts of interest

The authors declare the following competing financial interest. A patent application has been filed on 'Dibenzopyridoquinoxaline based derivatives' with A. Patra, B. Sk, M. Sarkar, and S. Kundu as inventors.

Acknowledgments

The infrastructural support from IISERB, financial support from BRNS, DAE (No. 37(2)/14/06/2016BRNS/37020), and Council of Scientific and Industrial Research (CSIR), New Delhi, (No. 01(2878)/17/EMR-II) is gratefully acknowledged. BSk and SK thank IISERB and UGC, respectively, for fellowship. We thank Ms. Ashima Negi and Dr. A. Gupta at IISERB for helping to record decays using iCCD camera, Dr. Jogendar Singh at IISERB, and Dr. J. A. Mondal at BARC for fruitful discussion.

View Article Online
DOI: 10.1039/D0TC02520H

Notes and references

1. M. Lor, J. Thielemans, L. Viaene, M. Cotlet, J. Hofkens, T. Weil, C. Hampel, K. Müllen, J. W. Verhoeven, M. V. Auweraer and F. C. D. Schryver, *J. Am. Chem. Soc.*, 2002, **124**, 9918-9925.
2. H. Uoyama, K. Goushi, K. Shizu, H. Nomura and C. Adachi, *Nature*, 2012, **492**, 234.
3. K. Kawasumi, T. Wu, T. Y. Zhu, H. S. Chae, T. V. Voorhis, M. A. Baldo and T. M. Swager, *J. Am. Chem. Soc.*, 2015, **137**, 11908-11911.
4. S. Feuillastre, M. Pauton, L. H. Gao, A. Desmarchelier, A. J. Riives, D. Prim, D. Tondelier, B. Geffroy, G. Muller, G. Clavier and G. Pieters, *J. Am. Chem. Soc.*, 2016, **138**, 3990-3993.
5. D. M. E. Freeman, A. J. Musser, J. M. Fros, H. L. Stern, A. K. Forster, K. J. Fallon, A. G. Rapidis, F. Cacialli, I. McCulloch, T. M. Clarke, R. H. Friend and H. Bronstein, *J. Am. Chem. Soc.*, 2017, **139**, 11073-11080.
6. P. K. Samanta, D. Kim, V. Coropceanu and J. L. Bredas, *J. Am. Chem. Soc.*, 2017, **139**, 4042-4051.
7. A. B. Pun, S. N. Sanders, E. Kumarasamy, M. Y. Sfeir, D. N. Congreve and L. M. Campos, *Adv. Mater.*, 2017, **29**, 1701416.
8. C. J. Chen, R. J. Huang, A. S. Batsanov, P. Pander, Y. T. Hsu, Z. G. Chi, F. B. Dias and M. R. Bryce, *Angew. Chem. Int. Ed.*, 2018, **57**, 16407-16411.
9. S. Kundu, B. Sk, P. Pallavi, A. Giri and A. Patra, *Chem. Eur. J.*, 2020, **26**, 5557-5582.
10. J. M. Lupton, A. Pogantsch, T. Piok, E. J. W. List, S. Patil and U. Scherf, *Phys. Rev. Lett.*, 2002, **89**, 4.
11. H. Tanaka, K. Shizu, H. Nakanotani and C. Adachi, *Chem. Mater.*, 2013, **25**, 3766-3771.
12. J. S. Ward, R. S. Nobuyasu, A. S. Batsanov, P. Data, A. P. Monkman, F. B. Dias and M. R. Bryce, *Chem. Commun.*, 2016, **52**, 2612-2615.
13. M. Louis, H. Thomas, M. Gmelch, A. Haft, F. Fries and S. Reineke, *Adv. Mater.*, 2019, **31**, 1807887.
14. L. Zhan, Z. Chen, S. Gong, Y. Xiang, F. Ni, X. Zeng, G. Xie and C. Yang, *Angew. Chem. Int. Ed.*, 2019, **58**, 17651-17655.
15. J. Yuan, R. Chen, X. Tang, Y. Tao, S. Xu, L. Jin, C. Chen, X. Zhou, C. Zheng and W. Huang, *Chem. Sci.*, 2019, **10**, 5031-5038.
16. F. B. Dias, K. N. Bourdakos, V. Jankus, K. C. Moss, K. T. Kamtekar, V. Bhalla, J. Santos, M. R. Bryce and A. P. Monkman, *Adv. Mater.*, 2013, **25**, 3707-3714.
17. H. Liu, Y. Gao, J. Cao, T. Li, Y. Wen, Y. Ge, L. Zhang, G. Pan, T. Zhou and B. Yang, *Mater. Chem. Front.*, 2018, **2**, 1853-1858.
18. Z. An, C. Zheng, Y. Tao, R. Chen, H. Shi, T. Chen, Z. Wang, H. Li, R. Deng, X. Liu and W. Huang, *Nat. Mater.*, 2015, **14**, 685.
19. M. Gmelch, H. Thomas, F. Fries and S. Reineke, *Sci. Adv.*, 2019, **5**, eaau7310.
20. H. Shi, L. Song, H. Ma, C. Sun, K. Huang, A. Lv, W. Ye, H. Wang, S. Cai, W. Yao, Y. Zhang, R. Zheng, Z. An and W. Huang, *J. Phys. Chem. Lett.*, 2019, **10**, 595-600.
21. X. Xiong, F. Song, J. Wang, Y. Zhang, Y. Xue, L. Sun, N. Jiang, P. Gao, L. Tian and X. Peng, *J. Am. Chem. Soc.*, 2014, **136**, 9590-9597.
22. Z. He, H. Gao, S. Zhang, S. Zheng, Y. Wang, Z. Zhao, D. Ding, B. Yang, Y. Zhang and W. Z. Yuan, *Adv. Mater.*, 2019, **31**, 1807222.
23. M. A. El-Sayed, *J. Chem. Phys.*, 1963, **38**, 2834-2838.
24. H. Ma, Q. Peng, Z. An, W. Huang and Z. Shuai, *J. Am. Chem. Soc.*, 2019, **141**, 1010-1015.
25. H. Noda, X. Chen, H. Nakanotani, T. Hosokai, M. Miyajima, N. Notsuka, Y. Kashima, J. Brédas and C. Adachi, *Nat. Mater.*, 2019, **18**, 1084-1090.
26. P. Sudhakar and T. P. Radhakrishnan, *J. Mater. Chem. C*, 2019, **7**, 7083-7089.
27. I. Bhattacharjee, N. Acharya, H. Bhatia and D. Ray, *J. Phys. Chem. Lett.*, 2018, **9**, 2733-2738.
28. L. Huang, L. Liu, X. Li, H. Hu, M. Chen, Q. Yang, Z. Ma and X. Jia, *Angew. Chem. Int. Ed.*, 2019, **58**, 16445-16450.
29. H. Wu, L. Gu, G. V. Baryshnikov, H. Wang, B. F. Minaev, H. Agren and Y. Zhao, *ACS Appl. Mater. Interfaces*, 2020, **12**, 20765-20774.
30. C. S. Oh, D. S. Pereira, S. H. Han, H. J. Park, H. F. Higginbotham, A. P. Monkman and J. Y. Lee, *ACS Appl. Mater. Interfaces*, 2018, **10**, 35420-35429.
31. J. Lin, S. Li, Z. Liu, D. Chen, C. Huang, Y. Wei, Y. Chen, Z. Tsai, C. Lo, W. Hung, K. Wong and P. Chou, *Chem. Mater.*, 2019, **31**, 5981-5992.
32. J. Liu, T. Hu, Z. Li, X. Wei, X. Hu, H. Gao, G. Liu, Y. Yi, Y. Yamada-Takamura, C. Lee, P. Wang and Y. Wang, *J. Phys. Chem. Lett.*, 2019, **10**, 1888–1893.
33. N. A. Kukhta, R. Huang, A. S. Batsanov, M. R. Bryce and F. B. Dias, *J. Phys. Chem. C*, 2019, **123**, 26536-26546.
34. B. Sk, S. Khodia and A. Patra, *Chem. Commun.*, 2018, **54**, 1786-1789.
35. F. Xie, H. Li, G. Dai, Y. Li, T. Cheng, M. Xie, J. Tang and X. Zhao, *ACS Appl. Mater. Interfaces*, 2019, **11**, 26144-26151.
36. G. Gokce, B. Karabay, A. Cihaner and M. I. Ozkut, *J. Polym. Sci. Part A: Polym. Chem.*, 2017, **55**, 3483-3493.
37. H. Jiang, Y. Wu, A. Islam, M. Wu, W. Zhang, C. Shen, H. Zhang, E. Li, H. Tian and W. Zhu, *ACS Appl. Mater. Interfaces*, 2018, **10**, 13635-13644.
38. R. Pashazadeh, P. Pander, A. Bucinskas, P. J. Skabara, F. B. Dias and J. V. Grazulevicius, *Chem. Commun.*, 2018, **54**, 13857-13860.
39. Z. Zhang, Y. Wu, K. Tang, C. Chen, J. Ho, J. Su, H. Tian and P. Chou, *J. Am. Chem. Soc.*, 2015, **137**, 8509-8520.
40. P. Data, P. Pander, M. Okazaki, Y. Takeda, S. Minakata and A. P. Monkman, *Angew. Chem. Int. Ed.*, 2016, **55**, 5739-5744.
41. Y. Im, M. Kim, Y. J. Cho, J. Seo, K. S. Yook and J. Y. Lee, *Chem. Mater.*, 2017, **29**, 1946-1963.
42. J. R. Lakowicz, *Principles of fluorescence spectroscopy*, Springer, New York, 2006.
43. B. Dereka, A. Rosspeintner, R. Stezycki, C. Ruckebusch, D. T. Gryko and E. Vauthey, *J. Phys. Chem. Lett.*, 2017, **8**, 6029-6034.
44. S. Singha, D. Kim, B. Roy, S. Sambasivan, H. Moon, A. S. Rao, J. Y. Kim, T. Joo, J. W. Park, Y. M. Rhee, T. Wang, K. H. Kim, Y. H. Shin, J. Jung and K. H. Ahn, *Chem. Sci.*, 2015, **6**, 4335-4342.
45. M. Collot, S. Bou, T. K. Fam, L. Richert, Y. Mely, L. Danglot and A. S. Klymchenko, *Anal. Chem.*, 2019, **91**, 1928-1935.
46. T. Suhina, S. Amirjalayer, B. Mennucci, S. Woutersen, M. Hilbers, D. Bonn and A. M. Brouwer, *J. Phys. Chem. Lett.*, 2016, **7**, 4285-4290.
47. Y. Wang, J. Yang, Y. Tian, M. Fang, Q. Liao, L. Wang, W. Hu, B. Z. Tang and Z. Li, *Chem. Sci.*, 2020, **11**, 833–838.
48. F. Ni, Z. Zhu, X. Tong, M. Xie, Q. Zhao, C. Zhong, Y. Zou and C. Yang, *Chem. Sci.*, 2018, **9**, 6150-6155.
49. T. Chen, L. Zheng, J. Yuan, Z. An, R. Chen, Y. Tao, H. Li, X. Xie and W. Huang, *Sci. Rep.*, 2015, **5**, 10923.
50. A. Forni, E. Lucenti, C. Botta and E. Cariati, *J. Mater. Chem. C*, 2018, **6**, 4603-4626.
51. J. Yang, X. Zhen, B. Wang, X. Gao, Z. Ren, J. Wang, Y. Xie, J. Li, Q. Peng, K. Pu and Z. Li, *Nat. Commun.*, 2018, **9**, 840.
52. J. Jin, H. Jiang, Q. Yang, L. Tang, Y. Tao, Y. Li, R. Chen, C. Zheng, Q. Fan, K. Y. Zhang, Q. Zhao and W. Huang, *Nat. Commun.*, 2020, **11**, 842.
53. J. Ye, L. Wang, H. Wang, H. Xie and Y. Qiu, *Org. Electron.*, 2019, **70**, 193-204.
54. Z. He, H. Gao, S. Zhang, S. Zheng, Y. Wang, Z. Zhao, D. Ding, B. Yang, Y. Zhang and W. Z. Yuan, *Adv. Mater.*, 2019, **31**, 1807222.
55. Y. Duan, L. Wen, Y. Gao, Y. Wu, L. Zhao, Y. Geng, G. Shan, M. Zhang and Z. Su, *J. Phys. Chem. C*, 2018, **122**, 23091-23101.

View Article Online
DOI: 10.1039/D0TC02520H

56 Y. Kitamoto, T. Namikawa, T. Suzuki, Y. Miyata, H. Kita, T. Sato and S. Oi, *Org. Electron.*, 2016, **34**, 208-217.
57 Z. He, W. Zhao, J. W. Y. Lam, Q. Peng, H. Ma, G. Liang, Z. Shuai and B. Z. Tang, *Nat. Commun.*, 2017, **8**, 416.
58 P. Pallavi, B. Sk, P. Ahir and A. Patra, *Chem. Eur. J.,* 2018, **24**, 1151-1158.

View Article Online
DOI: 10.1039/D0TC02520H

Graphical Abstract - Table of Content

“N-rich electron acceptors: triplet harvesting in multichromophoric pyridoquinoxaline and pyridopyrazine-based organic emitters”

By Bahadur Sk, Samarth Sharma, Anto James, Subhankar Kundu and Abhijit Patra*

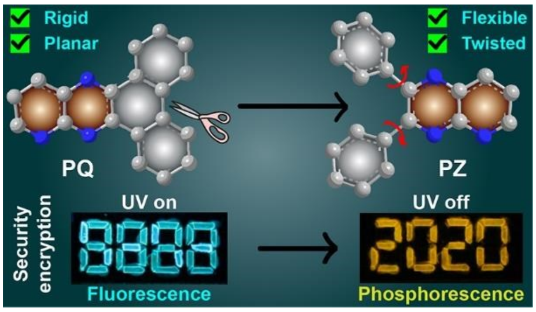

The role of rigid and flexible N-rich electron acceptor cores for the harvesting of triplet states through TADF and RTP was elucidated in a series of all-organic tridonor-acceptor compounds.